Suborbital measurements of spectral aerosol optical depth and its variability at sub-satellite-grid scales in support of CLAMS, 2001

J. Redemann[1], B. Schmid[1], J.A. Eilers[2], R. Kahn[3], R.C. Levy[4,5], P.B. Russell[2], J.M. Livingston[6], P.V. Hobbs[7], W.L. Smith Jr.[8], B.N. Holben[4]

[1]Bay Area Environmental Research Institute, Sonoma, CA

[2]NASA Ames Research Center, Moffett Field, CA

[3]Jet Propulsion Laboratory, Pasadena, CA

[4]NASA/Goddard Space Flight Center, Greenbelt, MD

[5]Also at Science Systems and Applications Inc., Lanham, MD

[6]SRI International, Menlo Park, CA

[7]University of Washington, Seattle, WA

[8]NASA Langley Research Center, Hampton, VA

Corresponding Author: Jens Redemann
BAERI/NASA Ames Research Center
MS 245-5
Moffett Field CA 94035-1000
Ph.: (805) 658-2637
Fax: (805) 658-2637
e-mail: jredemann@mail.arc.nasa.gov

For publication, Section "Articles", Journal of the Atmospheric Sciences, Special Issue: "Chesapeake Lighthouse and Aircraft Measurements for Satellites (CLAMS) Field Experiment"

November 10, 2003

Abstract

As part of the Chesapeake Lighthouse and Aircraft Measurements for Satellites (CLAMS) experiment, July 10 - August 2, 2001, off the central east coast of the United States, the 14-channel NASA Ames Airborne Tracking Sunphotometer (AATS-14) was operated aboard the University of Washington's Convair-580 research aircraft during 10 flights (~45 flight hours). One of the main research goals in CLAMS was the validation of satellite-based retrievals of aerosol properties. The goal of this study in particular was to perform true over-ocean validations (rather than over-ocean validation with ground-based, coastal sites) at finer spatial scales and extending to longer wavelengths than those considered in previous studies. Comparisons of AOD between the AERONET Cimel instrument at the Chesapeake Lighthouse and airborne measurements by AATS-14 in its vicinity showed good agreement with the largest r-square correlation coefficients at wavelengths of 0.38 and 0.5 μm (>0.99). Coordinated low-level flight tracks of the Convair-580 during Terra overpass times permitted validation of over-ocean MODIS level 2 (MOD04_L2) multi-wavelength AOD data (10x10km, nadir) in 16 cases on three separate days. While the correlation between AATS-14 and MODIS-derived AOD was weak with an r-square of 0.55, almost 75% of all MODIS AOD measurements fell within the prelaunch estimated uncertainty range $\Delta\tau=\pm 0.03\pm 0.05\tau$. This weak correlation may be due to the small AODs (generally less than 0.1 at 0.5μm) encountered in these comparison cases. An analogous coordination exercise resulted in seven coincident over-ocean match-ups between AATS-14 and MISR measurements. The comparison between AATS-14 and the MISR standard algorithm regional mean AODs showed a stronger correlation with an r-square of 0.94. However, MISR AODs were systematically larger

than the corresponding AATS values, with an rms difference of ~0.06. AATS data collected during nine extended low-level Convair-580 flight tracks were used to assess the spatial variability in AOD at horizontal scales up to 100 km. At UV and mid-visible wavelengths, the largest absolute gradients in AOD were 0.1-0.2 per 50 km horizontal distance. In the near IR, analogous gradients rarely reached 0.05. On any given day, the relative gradients in AOD were remarkably similar for all wavelengths, with maximum values of 70% per 50 km and more typical values of 25%. The implications of these unique measurements of AOD spatial variability for common validation practices of satellite data products and for comparisons to large-scale aerosol models are discussed.

1. Introduction

The CLAMS (Lighthouse and Aircraft Measurements for Satellites) campaign was a clear sky, shortwave (SW) closure campaign and entailed measurements from the Chesapeake Lighthouse research platform (hereafter called COVE – CERES Ocean Validation Experiment), several land sites, 6 research aircraft and the Terra satellite [*Smith et al*., 2003]. CLAMS research goals included validation of satellite-based retrievals of aerosol properties, vertical profiles of radiative fluxes, temperature and water vapor. Suborbital measurements of aerosol optical depth (AOD) and columnar water vapor (CWV) were carried out at several AERONET (Aerosol Robotic Network) sites [*Holben et al*., 1998] and aboard five of the six airborne platforms using a variety of techniques. The University of Washington's Convair-580 research aircraft carried a suite of in situ instruments to characterize aerosol properties and the ambient radiation field [*Magi et al*., 2003]. Among the remote sensors aboard the Convair-580 was the NASA Ames Airborne Tracking Sunphotometer (AATS-14), which measures direct solar beam transmission through the atmosphere to determine AOD between 0.354 and 1.558 μm, as well as columnar water vapor.

Space-borne satellite sensors offer many potential advantages for studying aerosols at regional to global scales [*Kaufman et al.*, 2002; *Ramanathan et al*., 2001]. Among the sensors that have provided global aerosol information in the past are AVHRR (Advanced Very High Resolution Radiometer) and TOMS (Total Ozone Mapping Spectrometer), even though they were not optimized for the detection of aerosols. With the launch of the EOS Terra satellite in 1999, a new era of satellite-based observations of aerosols began. The MODIS (Moderate-resolution Imaging Spectroradiometer) instruments aboard the Terra and Aqua satellites [*Kaufman et al*., 1997] and the MISR (Multi-angle Imaging

Spectro-Radiometer) instrument [*Diner et al*., 1998, *Martonchik et al*., 1998] aboard Terra strive for improved radiometric calibration and are much more capable of detailed global aerosol observations. In the case of the MODIS instrument for example, the advantages of the new sensor include its improved spectral coverage, the narrower bandwidth of the individual channels, and improved spatial resolution of 500 m (250 m for some channels, compared to 1 km or 4 km for AVHRR and 50 km for TOMS). For MISR, the improved capabilities further stem from its multi-angle viewing technique, which results in the ability to separate surface from atmospheric properties and provides sensitivity to particle shape. In particular, the improved spatial resolution of the new sensors allows for a better detection and identification of clouds and hence an improved separation of aerosols from clouds.

Of considerable interest to satellite-based retrievals of aerosol optical depth is small-scale (a few hundred meters or less) variability. The question arises whether an average radiance in a given scene, as measured by a satellite sensor, can be readily translated into an average AOD over the scene. For example, in preliminary validation studies of the standard MISR AOD retrieval algorithm, *Kahn et al.* [2001a] found that over dark water pixel-to-pixel scene variability could contribute more to the aerosol optical depth retrieval uncertainty than uncertainties in the calibration of the MISR cameras. In the case of MODIS, spatial variability is of equally high importance. Both the MODIS over-ocean and over-land aerosol retrieval algorithms depend heavily on the spatial variability of radiances and hence also on the variability of aerosol fields in order to detect and mask cloudy pixels [*Remer et al*., 2003]. In the case of the land algorithm, the standard MODIS cloud mask may discard pixels that contain increased AOD in the immediate vicinity (<500m) of clouds. Also, the aerosol retrieval algorithm discards those pixels that have sufficient cloud contamination to place them in the upper 50% in terms of their

reflectance at 0.66μm. In the case of the ocean algorithm, cloud masking is based solely on the spatial variability of the reflectance at 0.55μm [*Martins et al*., 2002]. Hence, suborbital measurements of the actual spatial variability of AOD and tests of the impact of that variability on satellite radiances are crucial in assessing the adequacy of the aerosol retrieval algorithms and the cloud screening procedures used within them.

Spatial variability on the scale of a few hundred meters can only be assessed from suborbital platforms that move fast by comparison to wind advection speeds, and only with instruments that provide data at rates of a few Hz (1 Hz being equivalent to a spatial resolution of ~100 m at an aircraft speed of ~200 knots). Current airborne lidars are generally backscatter systems and as such deliver only limited qualitative information on aerosol variability, since the inversion of a backscatter lidar signal requires *a priori* knowledge of the extinction-to-backscatter (lidar) ratio [*Klett*, 1985]. When deployed on a fast-moving aircraft such as the Convair-580 during CLAMS, the NASA Ames Airborne Tracking Sunphotometers (AATS-6 and AATS-14) on the other hand provide the spatial resolution, data acquisition speed, and accuracy to support the overall goals of CLAMS and other satellite validation studies. Because the AATS instruments measure the direct solar beam transmission, and are hence unaffected by surface properties, they are excellent tools for studying the spatial variability of AOD and columnar water vapor on scales of a few hundred meters.

In this paper, we describe the AATS-14 measurements of AOD during the CLAMS experiment, with a special emphasis on assessing the spatial variability of AOD on sub-satellite-grid scales with a resolution of 100 m. We include validation measurements for the MODIS and MISR over-ocean AOD retrieval products. For MISR, the standard aerosol retrieval algorithm produces results for a grid of 16 x 16 pixels (17.6 x 17.6 km), while the most relevant grid size for MODIS validation efforts has been 5 x 5 level 2

boxes, resulting in a grid of 50 x 50 km at nadir. Hence, we assess AATS-14 derived AOD variability at and below these spatial scales, determining both the mean AOD at these scales as well as the maximum variability within the satellite grids. In addition, we present comparisons of AOD measurements by the airborne AATS-14 and by an AERONET Cimel sunphotometer stationed at the COVE (CERES Ocean Validation Experiment) platform (36.9N, 75.71W). We also analyze the AOD variability in the vicinity of the COVE site. In this way we assess the suitability of the COVE platform as a satellite validation site and support one of the overall goals of the CLAMS experiment, namely to determine how representative measurements at the COVE site may be of the satellite grids around it.

2. Instrumentation

2.1 NASA Ames Airborne Tracking Sunphotometer AATS-14

Similar to its predecessor AATS-6 [*Matsumoto et al*., 1987], AATS-14 measures direct solar beam transmission in narrow channels (2-5.6 nm for the wavelengths between 0.35 and 1.56μm and 17.3 nm for the 2.1μm channel) by using detectors in a tracking head that can rotate about two axes. Azimuth and elevation motors controlled by differential sun sensors rotate the tracking head, thereby locking on to the solar beam and keeping detectors normal to it. The instrument's tracking head mounts external to the aircraft skin, to minimize blockage by aircraft structures and also to avoid data contamination by aircraft-window effects. AATS-14 is designed to operate on a variety of aircraft, including remotely piloted. It can locate and track the sun without input from an operator and record data in a self-contained data system. Using aircraft-provided data on latitude, longitude and ambient static pressure, aerosol (or particulate) optical depth

$\tau_p(\lambda)$ and columnar water vapor (CWV) are computed in real-time and displayed at the operator station (along with raw data, instrument status, and aircraft-provided data). Radiometric calibration is determined from Langley plots [*Schmid and Wehrli*, 1995]. Vertical differentiation of AOD and CWV data in suitable flight patterns yields extinction spectra and water vapor concentration. Examples of measurements in previous deployments are given by *Russell et al*. [1999], *Schmid et al*. [2000], *Livingston et al*. [2003], and *Redemann et al*. [2003].

Our methods for data reduction, calibration, and error analysis have been described previously [*Russell et al*., 1993; *Schmid and Wehrli*, 1995; *Schmid et al*., 1998 and 2001]. A brief summary is given here. The AATS-14 channels are chosen to allow separation of aerosol, water vapor, and ozone transmission. From these slant-path transmissions we retrieve $\tau_p(\lambda)$ in 13 narrow wavelength bands and the columnar amounts of water vapor and ozone. In addition to corrections for Rayleigh scattering and O_3 absorption, some channels require corrections for NO_2, H_2O and O_2-O_2 absorption. Cross-sections were computed using LBLRTM 6.01 [*Clough and Iacono*, 1995] with the CKD 2.4.1 continuum model using the HITRAN 2000 (v 11.0) line-list [*Rothman et al., 2001, 2002*] (including an update for water vapor from 04/2001, see http://www.hitran.com/hitran/updates.html). NO_2 cross-sections not included in LBLRTM 6.01 were taken from *Harder et al*. [1997]. NO_2 was assumed constant at 2×10^{-15} molecules cm^{-2}. The CLAMS AATS-14 data set consists of 13 wavelengths (0.354, 0.380, 0.449, 0.499, 0.525, 0.606, 0.675, 0.778, 0.865, 1.019, 1.059, 1.241 and 1.558μm) at which we retrieve $\tau_p(\lambda)$ and the 0.94-μm wavelength, which we use to determine CWV [*Schmid et al*., 2001]. AATS-14 was calibrated at the Mauna Loa Observatory (MLO), Hawaii, in June and September of 2001 using the Langley plot

technique [*Schmid and Wehrli*, 1995], effectively bracketing the CLAMS campaign. As a result of band-pass filter degradation, the calibration constants obtained from the post-mission calibration were lower than those obtained from the pre-mission calibration. However, for seven of the 14 wavelengths the change was only 0.6% or less. Four of the remaining seven channels had degraded by less than 2% and the remaining three channels had degraded by 2.8 to 4%. Because we had no indication of an abrupt change in the calibration constants we used the average of the June and September calibration constants, effectively assuming that the calibration change happened gradually over time. We considered the change in calibration constants by including a statistical uncertainty in the calibration constants equal to half the range between pre- and post-mission calibration.

Because sunphotometers have a non-zero field of view (FOV), they measure some diffuse light in addition to the direct solar beam. As a result, uncorrected sunphotometer measurements can overestimate direct-beam transmission and hence underestimate $\tau_p(\lambda)$. This effect increases with decreasing wavelength and increasing particle size in the column. We estimated these diffuse light effects using formulations derived by *Russell et al.* [2003], which are applicable over a wide range of column particle size distributions containing large and small aerosol particles. However, because of the predominance of small particles in the CLAMS campaign, these diffuse light corrections were generally negligible.

2.2 MODIS retrievals of aerosol optical depth

The approach of the MODIS over-ocean algorithm for the retrieval of aerosol optical depth is similar to that of the land algorithm [*Tanré et al*., 1997], but the channels

used and other features are quite different [*Remer et al*., 2003]. In the first step, the reflectances from the six channels at 0.55, 0.66, 0.86, 1.24, 1.6 and 2.13 μm are grouped into nominal 10 km boxes of 20 by 20 pixels at 500 m resolution. The standard MOD35 cloud mask uses the brightness in the visible channels to identify clouds. This procedure will mistake heavy aerosol as cloudy, and can miss important aerosol events over the ocean [*Remer et al*., 2003, *Martins et al*., 2002]. On the other hand, relying solely on IR-tests permits low altitude, warm clouds to be misidentified as 'clear', introducing cloud contamination in the aerosol products. Thus, the cloud mask used in the MODIS aerosol retrieval algorithm is based on the difference in spatial variability between aerosols and clouds. It computes the standard deviation of 0.55μm reflectances in every group of 3 by 3 pixels within a box [*Martins et al*., 2002]. Any group of 9 contiguous pixels with standard deviation greater than 0.0025 is labeled as 'cloudy', and all 9 pixels in the group are discarded. This test separates aerosol from most cloud types, but may fail at the centers of large, thick clouds and with cirrus, both of which can be spatially homogeneous. It may also erroneously identify inhomogeneous aerosol fields (e.g., dust) as clouds. In an effort to avoid both scenarios, additional spectral dependence filters are applied.

Initial validation efforts of the MODIS level 2 aerosol data product (MOD04_L2) were carried out by *Remer et al.*, [2002] for the over-ocean products based on two months of AERONET data in 2000, and by *Chu et al*. [2002] for the over-land AOD based on three months of AERONET data also in 2000. Since then, *Levy et al*. [2003a] analyzed the performance of the over-ocean algorithm in the presence of dust, *Levy et al*. [2003b] studied the performance of the land and ocean algorithm in the context of CLAMS and *Remer et al.* [2003] presented a validation effort of both the land and ocean

algorithms based on two years of AERONET data. In the most comprehensive of these studies, *Remer et al.* [2003] found that one standard deviation of all MODIS AOD retrievals (when compared to AERONET AOD measurements) fall within the predicted uncertainty $\Delta\tau = \pm 0.03 \pm 0.05\tau$ over ocean and $\Delta\tau = \pm 0.05 \pm 0.15\tau$ over land. All these validation studies used the validation approach developed by *Ichoku et al.* [2002], which entails averaging the MODIS data over nominally 50 x 50 km boxes and averaging the AERONET measurements over 1h. In this paper, we will investigate the implications of spatial averaging in the standard MODIS validation approach in the vicinity of the COVE platform, which is used as an AERONET site for MODIS validation work.

2.3 MISR retrievals of aerosol optical depth

MISR produces 36 simultaneous views of Earth, in a combination of nine angles varying from +70˚ to –70˚ in the along-track direction, in each of four spectral bands centered at 0.446, 0.558, 0.672 and 0.867 μm [*Diner et al*., 1998]. It takes seven minutes for all nine MISR cameras to view a fixed line on the surface, which sets the effective temporal resolution for coincident observations. At mid-latitudes, all locations are imaged about once per week in Global Mode, providing 275 m resolution data in all four nadir channels, and in the red channels of the other eight cameras. The remaining 24 channels of data are averaged on board the spacecraft to 1.1 km resolution. For the five MISR event days during CLAMS (July 10, 17, 19, 26, and August 2), the COVE platform was also designated as a MISR Local Mode site, which means that over an area 300 km along-track and 360 km cross-track, MISR data were acquired at 275 m resolution in all 36 channels.

Pre-launch theoretical studies indicated that MISR spectral radiances, measured at precisely known air-mass factors ranging from one to three, could provide tight constraints on AOD over land and water. Along with the wide range of scattering angles sampled (about 50˚ to 160˚ at mid-latitudes), MISR offers constraints on particle shape, size distribution, and composition, particularly over dark, uniform ocean surfaces [*Kahn et al.,* 2001b; *Martonchik et al.,* 1998].

The present study is one of several that involve field measurements to assess the sensitivity of aerosol retrievals based on satellite multi-angle imaging. In addition, the assumptions made in the retrieval algorithm about aerosol component particle properties, scene variability, and other factors, must be critically tested and refined. Together with studies from ACE-Asia (Aerosol Characterization Experiment – Asia) and SAFARI (Southern African Regional Science Initiative), the current study is part of an ongoing MISR validation effort aimed at defining a few satellite scenes very carefully and in detail to then extrapolate the findings regarding the performance of the aerosol retrieval algorithm. Since scene variability was determined in pre-launch studies to contribute significantly to the uncertainties in the aerosol retrievals, and since AOD variability is one of the main contributors to scene variability over the ocean, the analysis of spatial variability of AOD at and below the MISR retrieval grid performed in this paper should support the assessment of the performance of the MISR aerosol retrieval algorithm.

3. Results

3.1 Comparisons of AOD from AATS-14 and AERONET at COVE

During CLAMS, the Convair-580 aircraft carrying AATS-14 flew in the vicinity of the heavily instrumented COVE platform site (36.9°N, 75.71°W) on eleven occasions.

Among the instrumentation stationed at COVE were an MPL (Micro-pulse lidar) [*Welton et al*., 2001] as well as an AERONET Cimel sunphotometer [*Holben et al*., 1998]. The Cimel sunphotometer was mounted 37 m above sea level. For one of the 11 Convair-580 flybys, July 26, AERONET was not able to measure AOD within 45 minutes of the flyby. The remaining ten occasions are opportunities to compare the AATS-14-derived AOD spectra to the AERONET-derived AOD spectra. It should be noted that among the seven AERONET wavelengths (0.34, 0.38, 0.44, 0.50, 0.67, 0.87 and 1.02μm) and the 13 AATS-14 AOD wavelengths (0.354, 0.380, 0.449, 0.499, 0.525, 0.606, 0.675, 0.778, 0.865, 1.019, 1.059, 1.241 and 1.558μm) provide five nearly exact AERONET/AATS-14 wavelength matchups at 0.38/0.38, 0.50/0.499, 0.67/0.675, 0.87/0.865 and 1.02/1.019μm. Figure 1 shows the comparisons of AERONET and AATS-14 derived AOD at the shortest two and the longest two wavelength pairs, with the 0.67/0.675 pair not shown for brevity and lack of information different from the other four wavelength pairs. The AATS-14 derived AODs are taken as averages of short time spans (usually less than 90 seconds) when the Convair-580 was closest to COVE, generally within 6 km and at flight altitudes below 80 m. It can be seen that AATS-14 and AERONET are generally well-correlated with r-square values of 0.958 at 1.02 μm increasing to 0.997 at 0.38 μm. The rms differences at the three shortest wavelengths are of the order of 10% (relative rms difference calculated as the rms difference divided by the mean AOD), yet the rms difference at 1.02 μm is larger, at about 20.8%. The AATS-14 AODs at 1.02μm are generally larger than the AERONET values by about 0.01, which is significant at this wavelength. Also shown in Figure 1 are "error"-bars on the AATS-14 AOD data, which depict minimum and maximum values retrieved within a 10 km radius (light blue) and 50 km radius (dark blue) of the COVE site. From the occasional location of these error bars

to the left of the actual data points, it can be seen that the AERONET COVE site was sometimes collocated with the maxima in the regional AOD fields.

To explore this phenomenon further, and to assess the adequacy of the COVE platform as a satellite validation site, Table 1 summarizes the spatial statistics of the AATS-14 derived AOD fields during nine low-level flight legs centered at or in the vicinity of COVE. Data are given for distances within 6, 17 and 50 km of COVE, respectively and for wavelengths of 0.354, 0.499, 0.865, 1.019 and 1.558 μm. Two cases included in the AATS-14/AERONET comparisons in Figure 1 are not shown in Table 1, since the flight legs for those comparisons were too short to study AOD variability on the spatial scales of interest. The case study for July 26 was added to Table 1, although there was no AERONET level 2 data to compare to AATS-14 in Figure 1. For each case study, Table 1 summarizes the mean (μ_s) and the standard variation (σ_s) of the five-wavelength AOD data within the three distances (6, 17 and 50 km) of COVE. Also shown are the percentage differences of the mean AODs at the two scales from the mean AOD closest to COVE, viz.:

$$\Delta\mu_s = \frac{\left|\mu_{s,<6km} - \mu_{s,<xkm}\right|}{\mu_{s,<6km}} \quad (1)$$

where $\mu_{s,<6km}$ denotes the mean AOD in the closest possible proximity to the COVE site (generally < 6 km) and x is either 17 or 50 km. Six of the nine low-level flight tracks that went into Table 1 are shown in Figure 2. From Table 1, it can be seen that in three cases (case 2, 3 and 6) the mean AODs changed significantly when the data was averaged over larger areas. For cases 2 and 6, the differences in mean AOD in the closest vicinity to COVE as compared to a 50 km radius often exceeded 20%. There was no significant wavelength dependence in the AOD differences.

When we compare the AOD data in going from the closest proximity to COVE to the 17 km radius, the standard deviations increases in 5 out of 9 cases and it is constant in the remaining 4. In going from the 17 km to the 50 km data, only 6 cases show data for both spatial scales. Out of those 6 cases, the standard deviations increases for 3 cases, stays constant for 2 cases and decreases for one case. Hence, in general, standard deviations of AATS-14 AOD data increases with increasing spatial scale up to 50 km.

Another way of looking at spatial variability is depicted in Figures 2 and 3. Figure 2 shows all Convair-580 low-level flight tracks that extended at least 20 km horizontally. In addition to seven low-level flight legs in the vicinity of COVE which satisfied this criterion, two more flight legs flown on July 12 and 23 are shown. Figure 3 shows both the absolute (left panels) and the relative (right panels) difference in AOD from the AOD at the starting point of the low-level flight leg as a function of the horizontal distance from that point. At the UV (0.354 μm) and the mid-visible (0.499 μm) wavelength, the largest absolute gradients in AOD were 0.1-0.2 per 50 km horizontal distance. At 1.019 and 1.558μm, analogous gradients rarely measured 0.05. Figure 3 also shows that the relative gradients in AOD were remarkably similar for all wavelengths, with maximum values of 70% per 50 km and more typical values of 25%. In order to estimate an average relative change per horizontal distance we performed least-square no-offset linear fits to the absolute values of AOD difference versus horizontal distance. The no-offset straight line fits to the relative AOD differences show slopes between 0.47 and 0.64, although the straight line fit is probably a poor approximation to the data as indicated by the low correlation coefficients.

3.2 Comparisons of AATS-14 and MODIS-derived over-ocean AOD

AATS-14's participation in CLAMS was intended to support the over-ocean AOD validation of MODIS and MISR on Terra. An additional objective of the MODIS team was the development of an in-glint retrieval algorithm for AOD and aerosol column absorption. Consequently, the Convair-580 aircraft carrying AATS-14 was frequently located in regions of MODIS glint during Terra overpass time. Therefore, only a few non-glint validation opportunities for the MODIS aerosol product (MOD04_L2) presented themselves. Here we summarize the MODIS/AATS-14 comparisons from three non-glint retrieval scenes on July 14, 23 and 31. The goal of this study is to perform true over-ocean validations (rather than over-ocean validation with ground-based, coastal sites) at finer spatial scales and extending to longer wavelengths than those considered in previous studies.

Figure 4 shows the location of the Convair-580 flight tracks relative to the MODIS level 2 data grids, which have a nominal grid size of 10x10 km in the nadir and stretch out toward the edges of the MODIS granules. As in Figure 2, data points in blue along the flight tracks indicate an AATS-14 measurement, while the data points in green indicate a successful AATS-14 AOD retrieval at an aircraft altitude below 80 m. Only one of the three cases (July14) was located in the vicinity of COVE; the other two cases were located over darker ocean water.

The three separate days provided a total of 16 exact matchups between AATS-14 and MOD04_L2, with AATS-14 measurements performed generally within 15 minutes of the Terra overpass time (see Figure 5). Out of the 16 matchups, five took place on July 14 (panels a-e), seven on July 23 (panels f-l) and four on July 31 (panels m-p). It is noteworthy that the AOD for all 16 cases was ≤ 0.1 at a wavelength of 0.5μm. Panels a-e of Figure 5 also show the AERONET retrieval of AOD, averaged over the two

AERONET level 2 retrievals at 15:38 and 15:53UT (Terra overpass at 15:41UT). It can be seen that the curvature of the MODIS and AATS-14 spectra are very similar and that all data agree within the error bars. Starting at a wavelength of 0.87 μm, however, the AERONET AOD are below the AATS-14 derived values, and MODIS values do not agree with AERONET values within the error bars. For the 7 cases on July 23 (panels f-e), the MODIS-derived AOD is generally below the AATS-14 derived values, but the two data sets again agree well within the error bars, even though the magnitude of AOD at 0.5 μm was only about 0.05. The four cases on July 31 exhibit the poorest agreement out of all three days. AATS-14 derived AOD for that day is only about half the MODIS-derived AOD at all wavelengths.

By fitting a quadratic function to AATS-14 derived ln(AOD) vs. ln(λ), we can extrapolate the data beyond the longest AATS-14 wavelength (1.558μm) to compare AATS data with the data at the longest MODIS wavelength of 2.14 μm. Using these quadratics for each case in Figure 5 also enables us to calculate AATS-14 AODs at the exact seven MODIS wavelengths (0.47, 0.55, 0.66, 0.87, 1.24, 1.64 and 2.14 μm). For the 16 matchups shown in Figure 5 this process yields 112 data pairs of MODIS and AATS-14 AOD. These data pairs are plotted in Figure 6, along with a least-square linear fit to the data and the MODIS pre-launch estimate of the over-ocean AOD error given by $\Delta\tau = \pm 0.03 \pm 0.05\tau$. It can be seen that while the fit and the correlation are relatively poor, only ~27% of all MODIS data points fall outside of the pre-launch error range.

3.3 Comparisons of AATS-14 and MISR-derived over-ocean AOD

On four days during CLAMS, MISR aboard Terra sampled the region around the COVE site in local mode, effectively increasing the spatial resolution of all 36 channels to

275 m. These days were July 10, 17, 26 and August 2. In addition, AirMISR flew aboard the NASA ER-2 aircraft and collected data in the vicinity of COVE on July 12 and 31. In this paper however, we will only present data from the standard MISR AOD algorithm, which retrieves AOD at a scale of 16x16 pixels (1.1 km each) resulting in a retrieval box of 17x17 km. On July 10, the Convair-580 aircraft was not cleared to take-off until after Terra overpass time, and hence did not collect collocated data with MISR. Figure 7 shows the location of the Convair-580 flight tracks on the other three days and the boxes for which the standard MISR AOD retrieval algorithm reported successful AOD retrievals. For the data on July 26, the MISR algorithm screened out all data collocated with the Convair-580 flight track (likely due to cloud contamination), reducing the number of days with useful comparisons to two. The gaps in the lower row of pixels on July 17 and August 2 are caused by the algorithm identifying those areas as shallow water (case 2).

Figure 8 shows the comparison of spectral AOD data from AATS-14 and MISR for seven pixels, five on July 17 and 2 on August 2. MISR data are given at 0.446, 0.558, 0.672 and 0.867μm. Also shown are the AERONET retrieval at COVE at 16:17UT on July 17 and at 16:09 on August 2. It should be noted however, that panel (a) represents the best spatial collocation of AATS-14 and MISR data with AERONET on July 17, and panel (f) represents the best collocation on August 2. The AOD on July 17 was among the highest measured during CLAMS, with values around 0.4-0.5 at 0.5 μm. Figure 9 shows the scatter plot of MISR versus AATS-14 derived AOD for all four MISR wavelengths and all seven retrieval boxes shown in Figure 8. The data show a strong correlation, with an r-square of 0.94, but with an rms difference of 0.06 (26%). The least-square linear fit yields a slope of 0.97 and an offset of 0.054. Since the standard MISR

AOD error is estimated to be 0.05, this causes a number of data points to lie outside the error range.

4. Conclusions

We carried out studies of the spatial variability of aerosol optical depth (AOD) off the US central east coast in July and August of 2001. Based on measurements in the vicinity of the COVE (CERES Ocean Validation Experiment) platform (36.9°N, 75.71°W), the spatial variability in AOD on scales of up to 100 km was assessed. During ten flybys of the UW Convair-580 aircraft at the COVE site, comparisons of AATS-14 and an AERONET Cimel sunphotometer located at COVE showed good agreement and high correlation coefficients (0.98 and higher) for wavelengths between 0.38 and 0.87 μm. At 1.02 μm, AATS-14 measured systematically higher AOD by about 0.01. The rms differences of greater than 20% between the two data sets at 1.02 μm suggest the inappropriate treatment of gaseous absorption in either retrieval algorithm or the possible poor calibration of the 1.02 μm channel in one of the two instruments. The AATS-14 measurements used in these comparisons were generally obtained in the immediate vicinity of the COVE-AERONET site, only allowing data that was measured within a distance of 6 km. Since the MODIS validation procedure is to average the AOD data from 5x5 pixels (nominally 50 x 50 km at nadir) centered at a given validation site we also sought to characterize the spatial variability in AOD on those scales. For that purpose we compared spatially-averaged mean AOD in the closest proximity of COVE and within 17 and 50 km distances, respectively. In three out of nine cases, the mean AODs within both the 17 and the 50 km radius were significantly different from the mean AOD at the closest proximity. This finding differs from previous findings of the spatial pattern of AOD based on MODIS data [*Ichoku et al.*, 2002], and it raises the question

whether spatial variability contributed to the remaining differences in previous comparison studies between MODIS and suborbital measurements of spectral AOD.

An analysis of the spatial variability of AOD data, including two flight legs not in the vicinity of COVE, showed that AOD can vary by as much as 50-70%, but more typically 25-30% over horizontal distances of 50 km. Note that this variability does not address the differences in spatial mean AODs, but rather only the possible maximum variations between quasi-instantaneous AOD measurements. Note also, that we found no spectral dependence of the relative variability in AOD. This suggests that the spatial variability in AOD off the US East coast is caused by the transport and diffusion of similar aerosol types rather than the mixing of aerosol types of different size and composition.

The comparisons of AATS-14 and MODIS-derived level 2 AOD data products in this study are different from previous AOD validation studies in that we (i) use single level 2 MODIS data boxes (10x10km at nadir), (ii) use suborbital data extending to a wavelength of 1.558μm to extrapolate to the longest MODIS wavelength at 2.14μm and (iii) perform validation over dark water by using airborne sunphotometer measurements. Because of different objectives for AATS-14 in CLAMS, only a limited number of these validation opportunities occurred, all of which took place with very small aerosol loadings and consequently low AODs of 0.1 or below in the mid-visible. The curvature of the MODIS-derived AOD spectra compared well with the shape of the AATS-14 derived AOD spectra, although there was a systematic difference between the two AOD data sets on any given day. The systematic nature of that difference may be due to the limited choice of aerosol models for the MODIS retrievals or possibly due to the assumptions regarding sea surface conditions. Overall, the MODIS-AATS-14 comparisons showed relatively weak correlations and rms differences of 0.03 (65%). Nonetheless, 73% of all

MODIS data points were within the pre-launch predicted error range of 0.03±0.05AOD. Hence, the present study represents a successful validation effort for the MODIS over-ocean AOD product.

The comparisons of AATS-14 and coincident standard MISR aerosol products for CLAMS show strong correlation, though the MISR values are systematically offset by 0.05-0.06 towards larger AOD at all wavelengths, consistent with MISR-AATS comparison results from ACE-Asia and SAFARI-2000. The MISR results used in this study indicate that a lack of small, spherical non-absorbing particles in an earlier version of the MISR standard aerosol retrieval algorithm, which made the spectral slope of the MISR results too shallow [*Schmid et al*., 2003] has been corrected. The offset is the subject of continuing analysis by the MISR team; the systematic nature of the difference, coupled with the high correlation, suggest the resolution of this issue will bring the two measurements into very tight agreement. Further comparisons between CLAMS AATS-14 and the higher resolution (275 m) MISR data are planned.

Acknowledgments

This research was supported by grants through the NASA New Investigator Program (NIP) in Earth Science, the NASA's Earth Observing System Inter-Disciplinary Science (EOS-IDS) Program, and NASA's Radiation Sciences Program (RSP). The participation of AATS-14 in CLAMS was made possible by a grant through the NASA EOS validation program. We thank Ms. S. Ramirez for help in producing the manuscript and figures.

References

Chu, D. A., Y. J. Kaufman, C. Ichoku, L. A. Remer, D. Tanré, and B. N Holben, Validation of MODIS aerosol optical depth retrieval over land, *Geophys. Res. Lett., 29*(12), 8007, doi:10.1029/2001GL013205, 2002.

Clough S. A., and M. J. Iacono, Line-by-line calculations of atmospheric fluxes and cooling rates II: Application to carbon dioxide, ozone, methane, nitrous oxide, and the halocarbons, *J. Geophys. Res., 100*, 16,519-16,535, 1995.

Diner, D.J., et al., Multiangle Imaging Spectroradiometer (MISR) description and experiment overview, *IEEE Trans. Geosci. Remote Sens., 36*, 1072-1087, 1998.

Harder J. W., J. W. Brault, P. V. Johnston, and G. H. Mount, Temperature dependent NO_2 cross sections at high spectral resolution, *J. Geophys. Res.*, *102*, 3861-3879, 1997.

Holben, B. N., T. F. Eck, I. Slutsker, D. Tanré, J. P. Buis, A. Setzer, E. Vermote, J. A. Reagan, Y. J. Kaufman, T. Nakajima, F. Lavenu, I. Jankowiak and A. Smirnov, AERONET - A federated instrument network and data archive for aerosol characterization, *Rem. Sens. Environ*., *66*, 1-16, 1998.

Ichoku, C., D. A. Chu, S. Mattoo, Y. J. Kaufman, L. A. Remer, D. Tanré, I. Slutsker, and B. Holben, A spatio-temporal approach for global validation and analysis of MODIS aerosol products, *Geophys. Res. Lett., 29*, 10.1029/2001GL013206, 2002.

Kahn, R., P. Banerjee, D. McDonald, and J. Martonchik, Aerosol Properties Derived from Aircraft Multi-angle Imaging Over Monterey Bay, *J. Geophys. Res., 106*, 11,977-11,995, 2001a.

Kahn, R., P. Banerjee, and D. McDonald, Sensitivity of multiangle imaging to natural mixtures of aerosols over ocean , *J. Geophys. Res., 106,* 18,219-18,238, 2001b.

Kaufman, Y. J., D. Tanré, L. A. Remer, E. Vermote, A. Chu, and B. N. Holben, Operational remote sensing of tropospheric aerosol over land from EOS moderate resolution imaging spectroradiometer, *J. Geophys. Res., 102*, 17,051-17,067, 1997.

Kaufmann, Y.J., D. Tanré, and O. Boucher, A satellite view of aerosols in the climate system, *Nature*, *419*, 215-223, 2002.

Klett, J. D., Lidar inversion with variable backscatter/extinction ratios, *Appl.Opt*., *24*, 1638-1643, 1985.

Levy, R. C., L. A. Remer, D. Tanré, Y. J. Kaufman, C. Ichoku, B. N. Holben, J. M. Livingston, P. B. Russell, and H. Maring, Evaluation of the Moderate-Resolution Imaging Spectroradiometer (MODIS) retrievals of dust aerosol over the ocean during PRIDE, *J. Geophys. Res., 108*(D19), 8594, doi:10.1029/2002JD002460, 2003a.

Levy, R.C., L.A. Remer, J.V. Martins, Y.J. Kaufman, A. Plana-Fattori, J. Redemann, and B. Wenny, Evaluation of the MODIS aerosol retrievals over ocean and land during CLAMS, submitted for publication, section "Articles", *JAS*, special issue: "Chesapeake Lighthouse and Aircraft Measurements for Satellites (CLAMS) Field Experiment", 2003b.

Livingston, J. M., et al., Airborne Sun photometer measurements of aerosol optical depth and columnar water vapor during the Puerto Rico Dust Experiment and comparison with land, aircraft, and satellite measurements, *J. Geophys. Res., 108*(D19), 8588, doi:10.1029/2002JD002520, 2003.

Magi, B., P. V. Hobbs, T. W. Kirchstetter, I. T. Novakov, D. A. Hegg, S. Gao, J. Redemann, and B. Schmid, Aerosol Properties and Chemical Apportionment of Aerosol Optical Depth at Locations off the United States East Coast in July and August, submitted for publication, section "Articles", *JAS*, special issue: "Chesapeake

Lighthouse and Aircraft Measurements for Satellites (CLAMS) Field Experiment", 2003.

Martins, J. V., D. Tanré, L. Remer, Y. Kaufman, S. Mattoo, and R. Levy, MODIS cloud screening for remote sensing of aerosols over oceans using spatial variability, *Geophys. Res. Lett., 29*(12), 8009, doi:10.1029/2001GL013252, 2002.

Martonchik, J.V., D.J. Diner, R. Kahn, M.M. Verstraete, B. Pinty, H.R. Gordon, and T.P. Ackerman, Techniques for the retrieval of aerosol properties over land and ocean using multiangle imaging, *IEEE Trans. Geosci. Remote Sens., 36*, 1212-1227, 1998.

Matsumoto, T., P. B. Russell, C. Mina, W. Van Ark and V. Banta, Airborne Tracking Sunphotometer. *J. Atmos. Ocean. Tech*., *4*, 336-339, 1987.

Ramanathan, V., P.J. Crutzen, J.T. Kiehl, and D. Rosenfeld, Aerosol, Climate and the Hydrological Cycle, *Science*, *294*, 2119-2124, 2001.

Redemann, J., S. J. Masonis, B. Schmid, T. L. Anderson, P. B. Russell, J. M. Livingston, O. Dubovik, and A. D. Clarke, Clear-column closure studies of aerosols and water vapor aboard the NCAR C-130 during ACE-Asia, 2001, *J. Geophys. Res., 108*(D23), 8655, doi:10.1029/2003JD003442, 2003.

Remer, L. A., D. Tanré, Y. J. Kaufman, C. Ichoku, S. Mattoo, R. Levy, D. A. Chu, B. Holben, O. Dubovik, A. Smirnov, J. V. Martins, R. R. Li and Z. Ahmad, Validation of MODIS aerosol retrieval over ocean, *Geophys. Res. Lett*., 29(12), 8008, doi:10.1029/2001GL013204, 2002.

Remer, L.A., Y. J. Kaufman, D. Tanré, S. Mattoo, D. A. Chu, J. V. Martins, R.-R. Li, C. Ichoku, R. C. Levy, R. G. Kleidman, T. F. Eck, E. Vermote, B. N. Holben, The MODIS Aerosol Algorithm, Products and Validation, submitted for publication, section "Articles", *JAS*, special issue: "Chesapeake Lighthouse and Aircraft Measurements for Satellites (CLAMS) Field Experiment", 2003.

Rothman L.S., K. Chance, J. Schroeder, and A. Goldman. New Edition of HITRAN Database. 11th ARM Science Team Meeting Proceedings, Atlanta, Georgia, March 19-23, 2001.

Rothman L.S., and J. Schroeder, Millenium HITRAN Compilation. 12th ARM Science Team Meeting Proceedings, St. Petersburg, Florida, April 8-12, 2002.

Russell, P. B., J. M. Livingston, E. G. Dutton, R. F. Pueschel, J. A. Reagan, T. E. Defoor, M. A. Box, D. Allen, P. Pilewskie, B. M. Herman, S. A. Kinne, and D. J. Hofmann, Pinatubo and pre-Pinatubo optical-depth spectra: Mauna Loa measurements, comparisons, inferred particle size distributions, radiative effects, and relationship to lidar data. *J. Geophys. Res*., *98*, 22,969-22,985, 1993.

Russell, P. B., J. M. Livingston, P. Hignett, S. Kinne, J. Wong, and P. V. Hobbs, Aerosol-induced radiative flux changes off the United States Mid-Atlantic coast, Comparison of values calculated from sunphotometer and in situ data with those measured by airborne pyranometer, *J. Geophys. Res., 104*, 2289-2307, 1999.

Russell, P. B., J. M. Livingston, O. Dubovik, S. A. Ramirez, J. Wang, J. Redemann, B. Schmid, M. Box, and B. N. Holben, Sunlight transmission through desert dust and marine aerosols: Diffuse light corrections to Sun photometry and pyrheliometry, submitted to *J. Geophys. Res*., 2003.

Schmid, B., and C. Wehrli, Comparison of sun photometer calibration by Langley technique and standard lamp, *Appl. Opt*., *34*, 4500-4512, 1995.

Schmid, B., P. R. Spyak, S. F. Biggar, C. Wehrli, J. Sekler, T. Ingold, C. Mätzler, and N. Kämpfer, Evaluation of the applicability of solar and lamp radiometric calibrations of a precision Sun photometer operating between 300 and 1025 nm, *Appl. Opt., 37*, 3923-3941, 1998.

Schmid, B., J. M. Livingston, P. B. Russell, P. A. Durkee, H. H. Jonsson, D. R. Collins, R. C. Flagan, J. H. Seinfeld, S. Gassó, D. A. Hegg, E. Öström, K. J. Noone, E. J. Welton, K. J. Voss, H. R. Gordon, P. Formenti, and M. O. Andreae, Clear sky closure studies of lower tropospheric aerosol and water vapor during ACE-2 using airborne sunphotometer, airborne in-situ, space-borne, and ground-based measurements, *Tellus*, *B 52*, 568-593, 2000.

Schmid, B., et al., Comparison of columnar water-vapor measurements from solar transmittance methods. *Appl. Opt., 40*, 1886-1896, 2001.

Schmid, B., et al., Coordinated airborne, spaceborne, and ground-based measurements of massive thick aerosol layers during the dry season in southern Africa, *J. Geophys. Res., 108*(D13), 8496, doi:10.1029/2002JD002297, 2003.

Smith Jr., W., T. P. Charlock, R. Kahn, J. V. Martins, P. V. Hobbs, L. A. Remer, An Overview of the Chesapeake Lighthouse and AIrcreaft Measurements for Satellites (CLAMS) Experiment, submitted for publication, section "Articles", *JAS*, special issue: "Chesapeake Lighthouse and Aircraft Measurements for Satellites (CLAMS) Field Experiment", 2003.

Tanré, D., Y. J. Kaufman, M. Herman and S. Mattoo, Remote sensing of aerosol properties over oceans using the MODIS/EOS spectral radiances. *J. Geophys. Res.-Atmos., 102*(14), 16971-16988, 1997.

Welton, E. J., J. R. Campbell, J. D. Spinhirne, and V. S. Scott, "Global monitoring of clouds and aerosols using a network of micro-pulse lidar systems", in Lidar Remote Sensing for Industry and Environmental Monitoring, U. N. Singh, T. Itabe, N. Sugimoto, (eds.), *Proc. SPIE, 4153*, 151-158, 2001.

Table Captions

Table 1. Comparison of AATS-14 AOD measurements for nine flight legs during CLAMS in the vicinity of COVE. Data are given for 5 wavelengths. For each wavelength the mean AOD is shown for three different spatial scales: '6km' – closest to COVE, '17km' – averaged over all data within a distance of 17 km from COVE, and '50km' - averaged over all data within a distance of 50 km from COVE. Standard deviations are given for all data within the respective spatial scales along with the relative differences of the mean AOD within the larger two scales compared to the mean AOD within the smallest scale (cf. equation 1). Relative differences larger than 5% are given in bold numbers.

Figure Captions

Figure 1. Comparison of aerosol optical depth (AOD) derived from the NASA Ames Airborne Tracking Sunphotometer (AATS-14) and the AERONET Cimel Sunphotometer at the COVE platform (36.9°N, 75.71°W). Data are shown for four wavelengths. AATS-14 data was taken during low-level flight legs at a distance less than 6 km from COVE and at flight altitudes below 80 m. The light and dark blue error bars on the AATS-14 data represent the maximum variability within a range of 17 and 50 km from COVE respectively.

Figure 2. Location of nine low-level flight legs of the University of Washington's Convair-580 research aircraft in CLAMS. Green points mark locations of successful AATS-14 retrievals of AOD at flight altitudes below 80 m. Blue points indicate cloud

contamination or a flight altitude above 80 m. The red square marks the location of the Chesapeake Lighthouse.

Figure 3. Spatial variability in AODs derived from AATS-14 during the nine low-level flight legs shown in Figure 2. Data are shown as absolute differences (left panels) and relative differences (right panels) from the AOD at the starting point of the low-level legs for four wavelengths (0.354, 0.499, 1.019 and 1.558 μm). The text in the legends gives the flight date and the starting point AOD for the respective legs.

Figure 4. Convair-580 flight tracks relative to the location of MODIS level 2 (MOD02_L2) aerosol retrieval boxes on July 14, 23 and 31. See Figure 2 for explanation of color code on the AATS-14 data points along the flight tracks.

Figure 5. Comparison of spectral AODs derived from AATS-14 and MODIS (MOD04_L2) for the 16 collocated measurements shown in Figure 4. Out of the 16 matchups, 5 took place on July 14 (panels a-e), 7 on July 23 (panels f-l) and 4 on July 31 (panels m-p). Also shown (as magenta triangles) are the AERONET AOD measurements at COVE closest in time to the Terra overpass time (as given in the title of each panel).

Figure 6. Scatter plot of AOD derived from AATS-14 and MODIS for seven wavelengths and the 16 matchups given in Figure 5. The 1:1 line is shown as a dashed line, while the solid black line represents the linear least-square fit to the data. The blue solid lines show the pre-launch estimated AOD uncertainty given by $\Delta\tau = \pm 0.03 \pm 0.05\tau$.

Figure 7. Convair-580 flight tracks relative to the location of the successful MISR standard retrieval algorithm boxes on July 17, 26 and August 2. See Figure 2 for explanation of color code on the AATS-14 data points along the flight tracks.

Figure 8. Comparison of spectral AODs derived from AATS-14 and the MISR standard algorithm (regional mean) for the 7 collocated measurements shown in Figure 7. Out of the 7 matchups, 5 took place on July 17 (panels a-e), and 2 on August 2 (panels f-g). Also shown (as magenta triangles) are the AERONET AOD measurements at COVE closest in time to the Terra overpass time (as given in the title of each panel).

Figure 9. Scatter plot of AATS-14 and regional mean MISR AOD (standard algorithm) for the four MISR wavelengths and the 7 matchups given in Figure 8. The 1:1 line is shown as a dashed line, while the solid black line represents the linear least-square fit to the data. The blue solid lines show the generic preliminary AOD uncertainty of 0.05.

Table 1.

Case		0.354μm			0.499μm			0.865μm			1.019μm			1.558μm		
		6km	17km	50km	6km	17km	50km	6km	17km	50km	6km	17km	50km	6km	17km	50km
1 July 10 18:23UT	μ_s	0.344	0.353	n/a	0.198	0.203	n/a	0.065	0.066	n/a	0.053	0.054	n/a	0.041	0.041	n/a
	σ_s	0.001	0.009	n/a	0.001	0.005	n/a	0.000	0.002	n/a	0.000	0.001	n/a	0.001	0.001	n/a
	$\mu_{s,<6km}$ [%]	n/a	2.8	n/a	n/a	2.6	n/a	n/a	2.3	n/a	n/a	2.1	n/a	n/a	1.2	n/a
2 July 10 18:58UT	μ_s	0.484	0.349	0.373	0.278	0.205	0.215	0.091	0.069	0.071	0.071	0.056	0.057	0.048	0.041	0.042
	σ_s	0.004	0.073	0.049	0.002	0.040	0.025	0.001	0.012	0.007	0.001	0.008	0.005	0.000	0.004	0.002
	$\mu_{s,<6km}$ [%]	n/a	**27.9**	**22.9**	n/a	**26.3**	**22.6**	n/a	**24.0**	**22.5**	n/a	**21.6**	**20.1**	n/a	**14.9**	**14.1**
3 July 14 15:34UT	μ_s	0.193	0.185	0.184	0.093	0.089	0.088	0.030	0.028	0.028	0.026	0.025	0.024	0.021	0.020	0.020
	σ_s	0.011	0.016	0.015	0.005	0.008	0.008	0.001	0.002	0.002	0.001	0.002	0.002	0.001	0.002	0.002
	$\mu_{s,<6km}$ [%]	n/a	4.0	4.4	n/a	4.4	4.9	n/a	**5.1**	**5.8**	n/a	4.7	**5.8**	n/a	**5.1**	**6.5**
4 July 17 16:12UT	μ_s	0.859	0.846	0.824	0.464	0.457	0.444	0.142	0.140	0.136	0.098	0.097	0.094	0.050	0.049	0.048
	σ_s	0.016	0.019	0.041	0.012	0.012	0.026	0.004	0.004	0.008	0.003	0.003	0.006	0.001	0.001	0.003
	$\mu_{s,<6km}$ [%]	n/a	1.5	4.1	n/a	1.6	4.4	n/a	1.4	4.3	n/a	1.4	4.5	n/a	1.6	4.8
5 July 17 16:32	μ_s	0.839	0.828	n/a	0.456	0.449	n/a	0.141	0.139	n/a	0.097	0.095	n/a	0.050	0.049	n/a
	σ_s	0.014	0.014	n/a	0.009	0.009	n/a	0.003	0.003	n/a	0.002	0.002	n/a	0.001	0.001	n/a
	$\mu_{s,<6km}$ [%]	n/a	1.3	n/a	n/a	1.6	n/a	n/a	1.6	n/a	n/a	2.0	n/a	n/a	2.0	n/a
6 July 26 15:55UT	μ_s	0.555	0.552	0.400	0.437	0.451	0.316	0.201	0.218	0.154	0.152	0.165	0.119	0.074	0.079	0.068
	σ_s	0.032	0.033	0.112	0.030	0.032	0.100	0.023	0.020	0.049	0.021	0.017	0.036	0.016	0.009	0.013
	$\mu_{s,<6km}$ [%]	n/a	0.6	**28.0**	n/a	3.3	**27.7**	n/a	**8.3**	**23.5**	n/a	**8.6**	**21.5**	n/a	**7.3**	**7.9**
7 Aug. 2 16:06UT	μ_s	0.197	0.200	0.205	0.103	0.105	0.108	0.036	0.037	0.037	0.030	0.030	0.031	0.021	0.022	0.022
	σ_s	0.004	0.010	0.013	0.002	0.005	0.007	0.001	0.001	0.002	0.000	0.001	0.001	0.000	0.001	0.001
	$\mu_{s,<6km}$ [%]	n/a	1.7	4.4	n/a	1.7	4.4	n/a	1.4	3.0	n/a	1.0	2.3	n/a	1.4	2.8
8 Aug. 2 16:22UT	μ_s	0.204	0.206	0.209	0.109	0.110	0.111	0.039	0.039	0.039	0.032	0.032	0.032	0.024	0.024	0.024
	σ_s	0.006	0.011	0.012	0.003	0.006	0.006	0.001	0.001	0.001	0.001	0.001	0.001	0.000	0.001	0.001
	$\mu_{s,<6km}$ [%]	n/a	1.2	2.5	n/a	1.0	2.0	n/a	0.5	0.5	n/a	0.0	0.0	n/a	0.0	0.4
9 Aug. 2 19:33UT	μ_s	0.228	0.226	n/a	0.123	0.122	n/a	0.044	0.043	n/a	0.036	0.036	n/a	0.029	0.029	n/a
	σ_s	0.006	0.005	n/a	0.003	0.003	n/a	0.001	0.001	n/a	0.001	0.001	n/a	0.001	0.001	n/a
	$\mu_{s,<6km}$ [%]	n/a	1.0	n/a	n/a	1.2	n/a	n/a	1.6	n/a	n/a	1.9	n/a	n/a	1.7	n/a

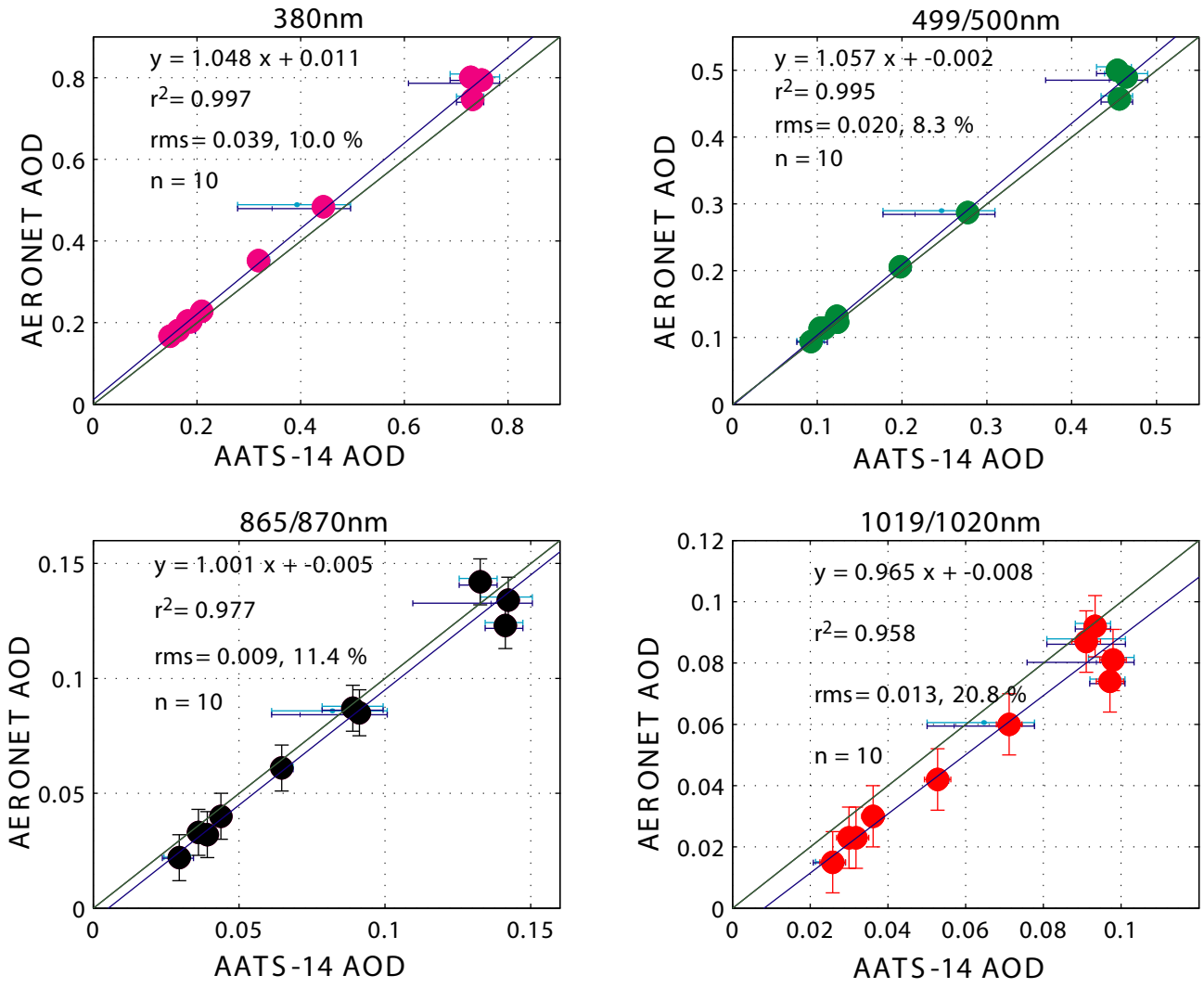

Figure 1. Comparison of aerosol optical depth (AOD) derived from the NASA Ames Airborne Tracking Sunphotometer (AATS-14) and the AERONET Cimel Sunphotometer at the COVE platform (36.9°N, 75.71°W). Data are shown for four wavelengths. AATS-14 data was taken during low-level flight legs at a distance less than 6 km from COVE and at flight altitudes below 80 m. The light and dark blue error bars on the AATS-14 data represent the maximum variability within a range of 17 and 50 km from COVE respectively.

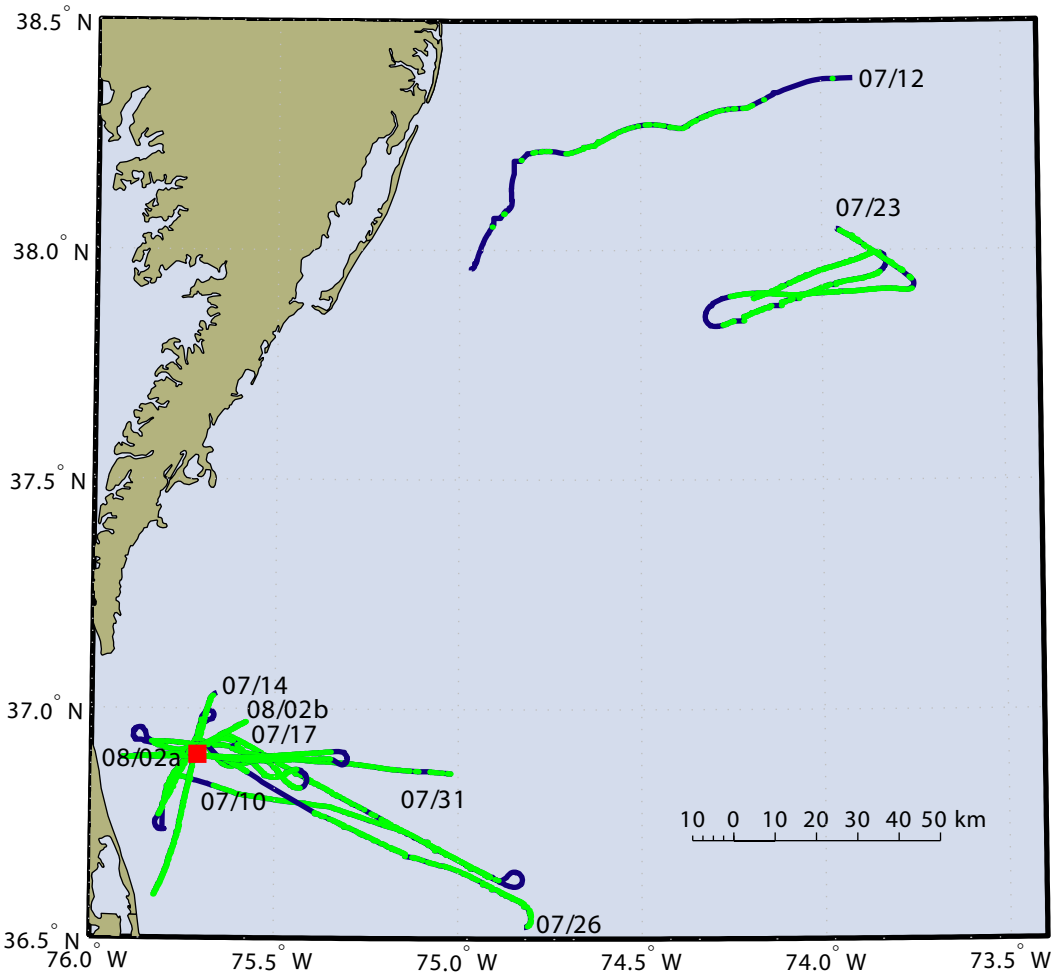

Figure 2. Location of nine low-level flight legs of the University of Washington's Convair-580 research aircraft in CLAMS. Green points mark locations of successful AATS-14 retrievals of AOD at flight altitudes below 80 m. Blue points indicate cloud contamination or a flight altitude above 80 m. The red square marks the location of the Chesapeake Lighthouse.

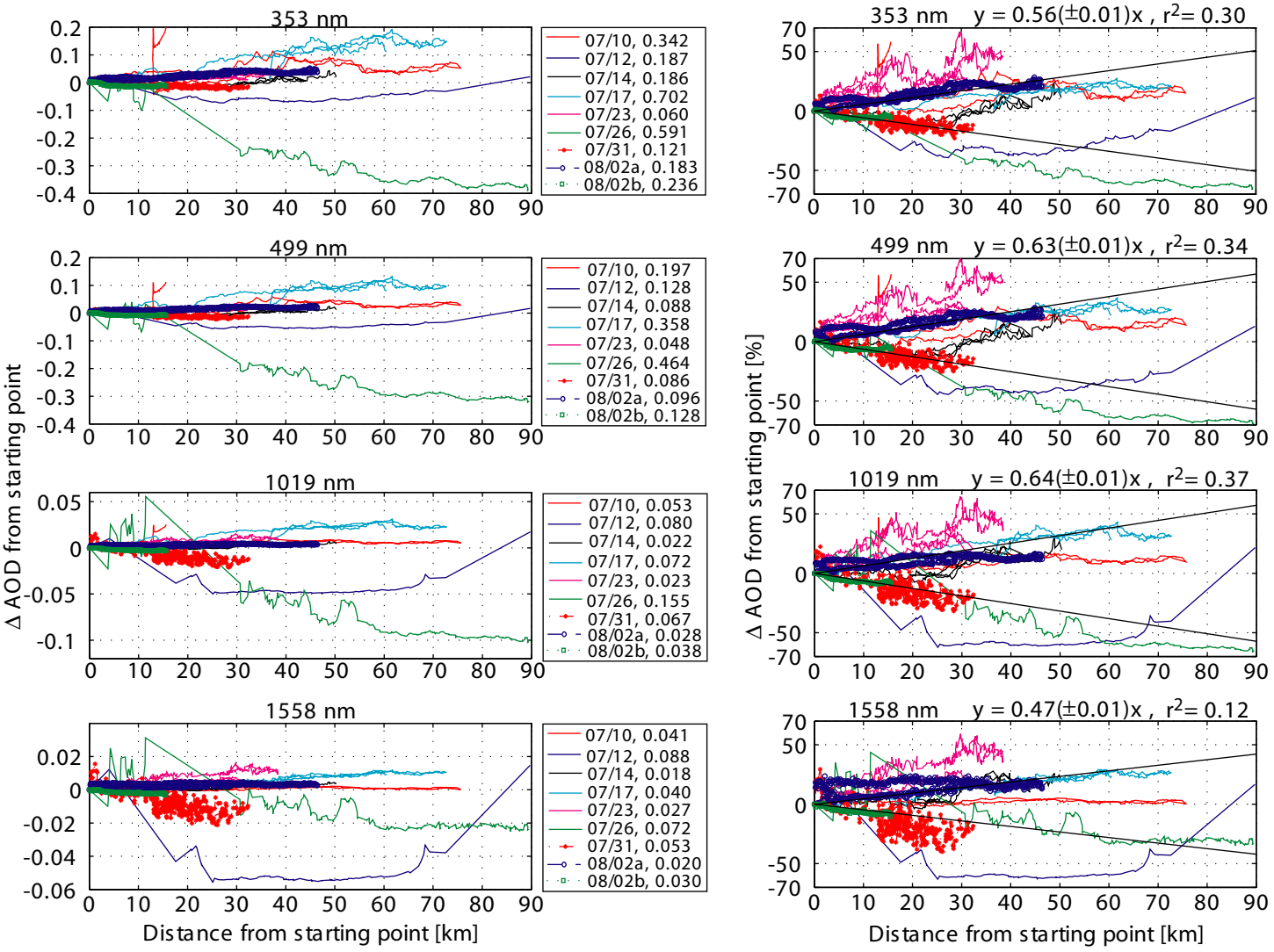

Figure 3. Spatial variability in AODs derived from AATS-14 during the nine low-level flight legs shown in Figure 2. Data are shown as absolute differences (left panels) and relative differences (right panels) from the AOD at the starting point of the low-level legs for four wavelengths (0.354, 0.499, 1.019 and 1.558 μm). The text in the legends gives the flight date and the starting point AOD for the respective legs.

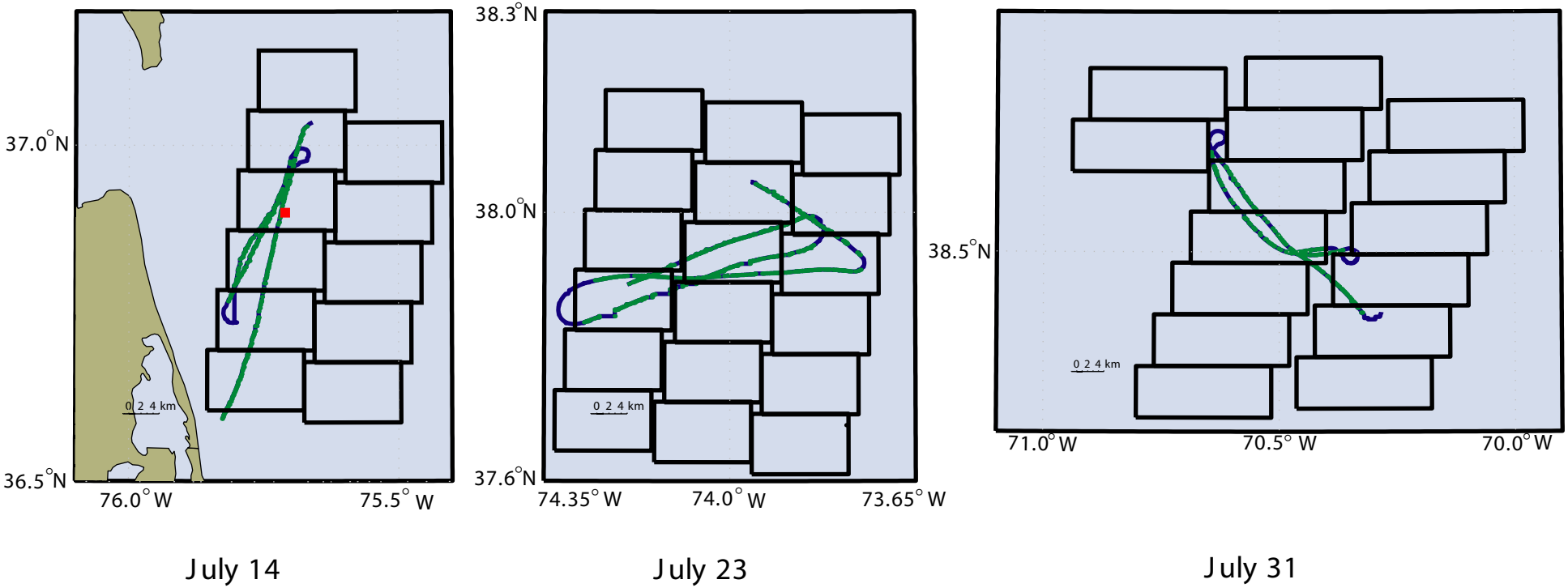

Figure 4. Convair-580 flight tracks relative to the location of MODIS level 2 (MOD02_L2) aerosol retrieval boxes on July 14, 23 and 31. See Figure 2 for explanation of color code on the AATS-14 data points along the flight tracks.

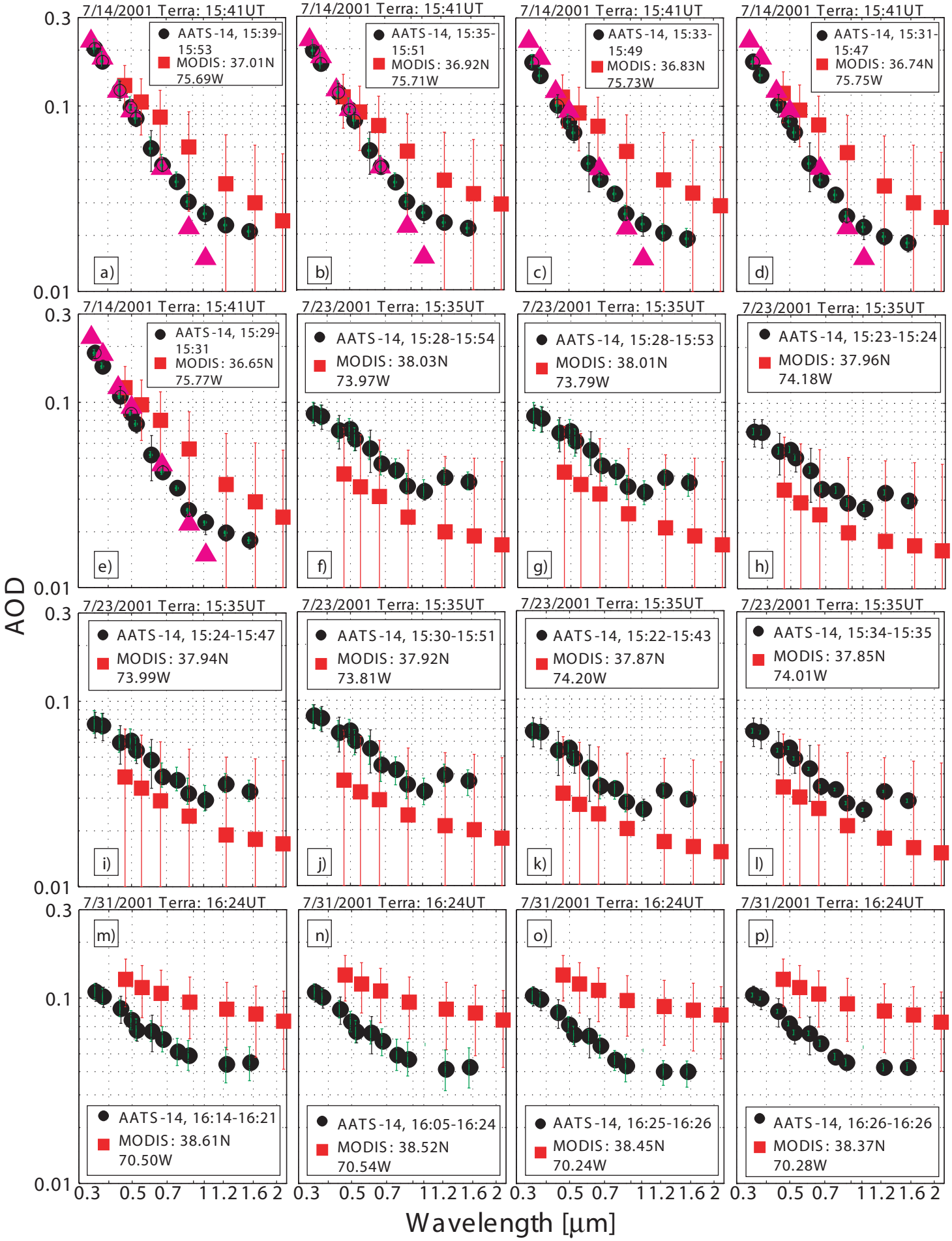

Figure 5. Comparison of spectral AODs derived from AATS-14 and MODIS (MOD04_L2) for the 16 collocated measurements shown in Figure 4. Out of the 16 matchups, 5 took place on July 14 (panels a-e), 7 on July 23 (panels f-l) and 4 on July 31 (panels m-p). Also shown (as magenta triangles) are the AERONET AOD measurements at COVE closest in time to the Terra overpass time (as given in the title of each panel).

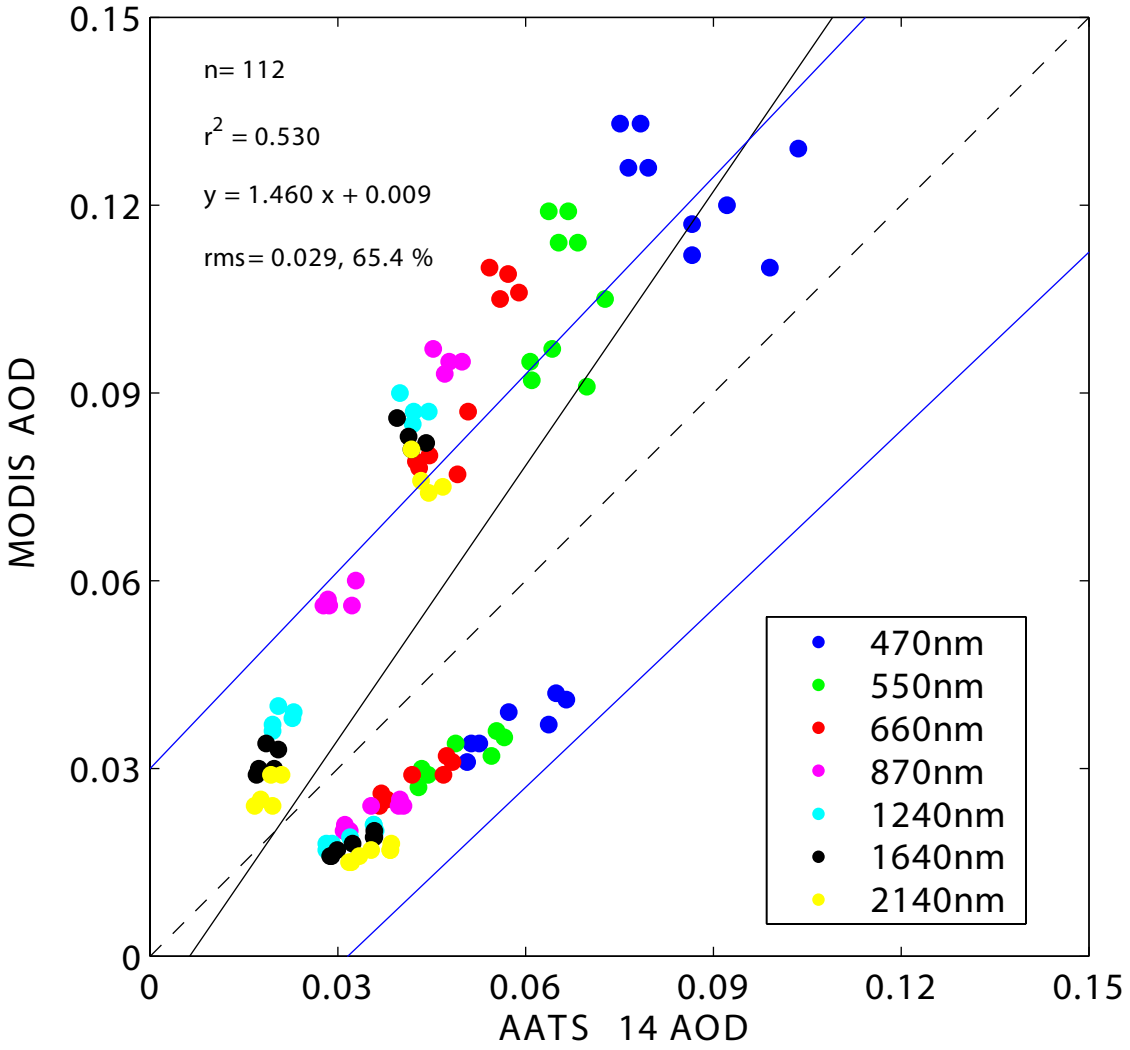

Figure 6. Scatter plot of AOD derived from AATS-14 and MODIS for seven wavelengths and the 16 matchups given in Figure 5. The 1:1 line is shown as a dashed line, while the solid black line represents the linear least-square fit to the data. The blue solid lines show the pre-launch estimated AOD uncertainty given by ±0.03±0.05AOD.

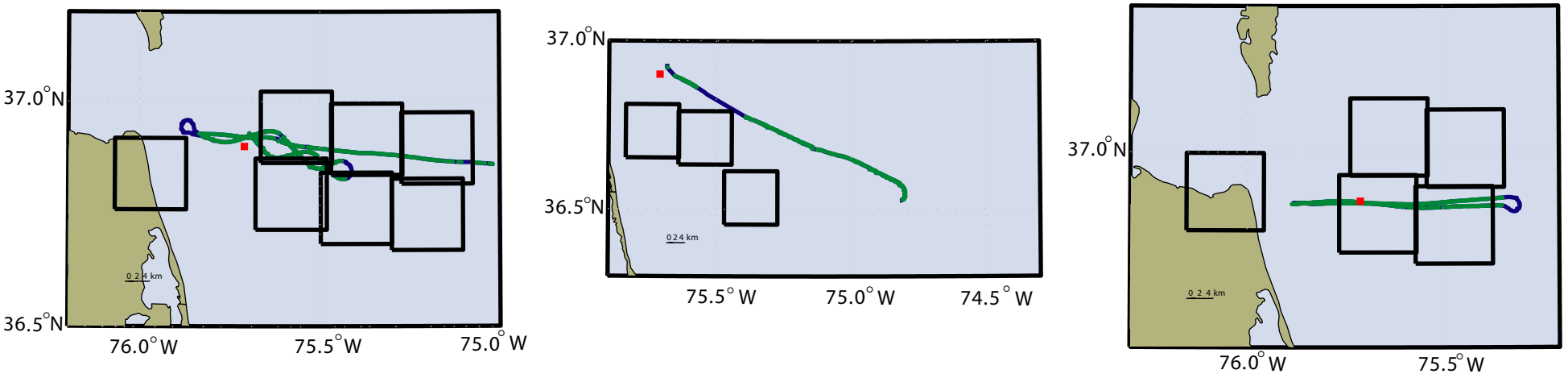

July 17 July 26 Aug. 02

Figure 7. Convair-580 flight tracks relative to the location of the successful MISR standard retrieval algorithm boxes on July 17, 26 and August 2. See Figure 2 for explanation of color code on the AATS-14 data points along the flight tracks.

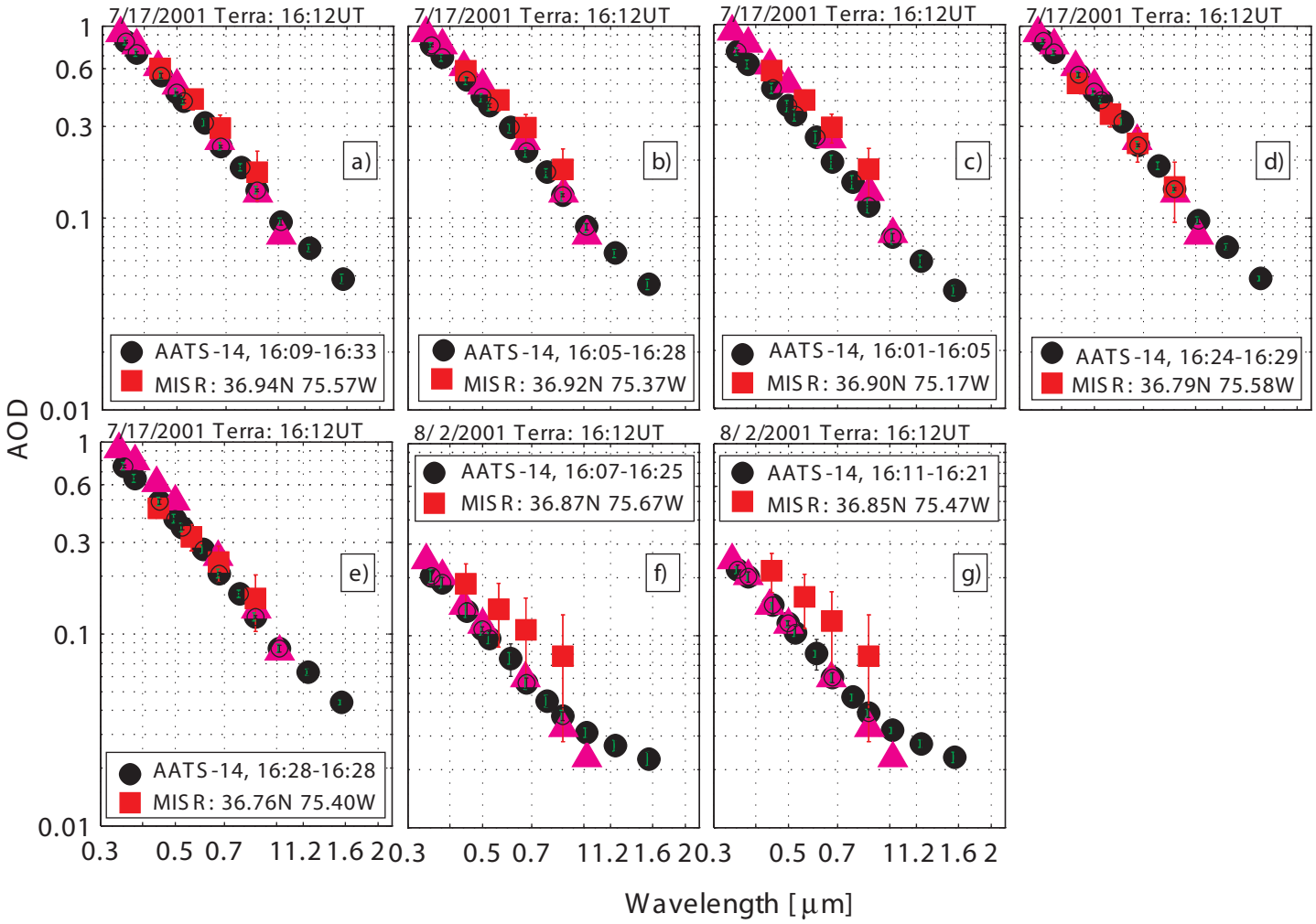

Figure 8. Comparison of spectral AODs derived from AATS-14 and the MISR standard algorithm (regional mean) for the 7 collocated measurements shown in Figure 7. Out of the 7 matchups, 5 took place on July 17 (panels a-e), and 2 on August 2 (panels f-g). Also shown (as magenta triangles) are the AERONET AOD measurements at COVE closest in time to the Terra overpass time (as given in the title of each panel).

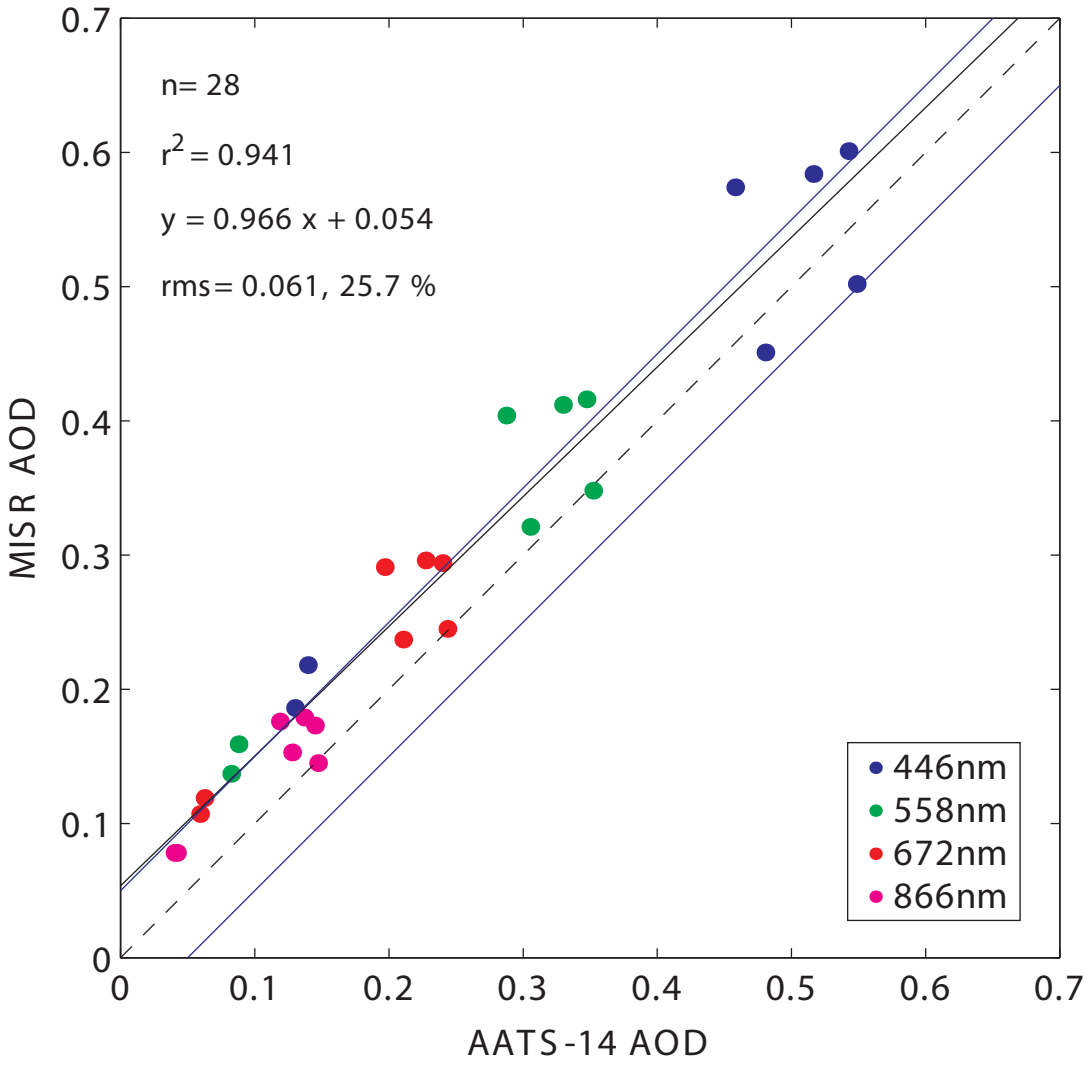

Figure 9. Scatter plot of AATS-14 and regional mean MISR AOD (standard algorithm) for the four MISR wavelengths and the 7 matchups given in Figure 8. The 1:1 line is shown as a dashed line, while the solid black line represents the linear least-square fit to the data. The blue solid lines show the generic preliminary AOD uncertainty of 0.05.